

Dark Distillation: Backdooring Distilled Datasets without Accessing Raw Data

Ziyuan Yang*

czyuanyang@gmail.com

Agency for Science, Technology and Research (A*STAR)
Singapore

Yi Zhang[†]

yzhang@scu.edu.cn

Sichuan University
China

Ming Yan

Yan_Ming@cfar.a-star.edu.sg

Agency for Science, Technology and Research (A*STAR)
Singapore

Joey Tianyi Zhou[†]

Joey_Zhou@cfar.a-star.edu.sg

Agency for Science, Technology and Research (A*STAR)
Singapore

Abstract

Dataset distillation (DD) is a powerful technique that enhances training efficiency and reduces transmission bandwidth by condensing large datasets into smaller, synthetic ones. It enables models to achieve performance comparable to those trained on the raw full dataset and has become a widely adopted method for data sharing. However, security concerns in DD remain underexplored. Existing studies typically assume that malicious behavior originates from dataset owners during the initial distillation process, where backdoors are injected into raw datasets. In contrast, this work is the first to address a more realistic and concerning threat: attackers may intercept the dataset distribution process, inject backdoors into the distilled datasets, and redistribute them to users. While distilled datasets were previously considered resistant to backdoor attacks, we demonstrate that they remain vulnerable to such attacks. Furthermore, we show that attackers do not even require access to any raw data to inject the backdoors successfully. Specifically, our approach reconstructs conceptual archetypes for each class from the model trained on the distilled dataset. Backdoors are then injected into these archetypes to update the distilled dataset. Moreover, we ensure the updated dataset not only retains the backdoor but also preserves the original optimization trajectory, thus maintaining the knowledge of the raw dataset. To achieve this, a hybrid loss is designed to integrate backdoor information along the benign optimization trajectory, ensuring that previously learned information is not forgotten. Extensive experiments demonstrate that distilled datasets are highly vulnerable to backdoor attacks, with risks pervasive across various raw datasets, distillation methods, and downstream training strategies. Moreover, our attack method is

highly efficient and lightweight, capable of synthesizing a malicious distilled dataset in under one minute in certain cases¹.

Keywords

Dataset Distillation, Backdoor Attack, Security Analysis, Deep Learning, Efficient Learning

ACM Reference Format:

Ziyuan Yang, Ming Yan, Yi Zhang, and Joey Tianyi Zhou. . Dark Distillation: Backdooring Distilled Datasets without Accessing Raw Data. In . ACM, New York, NY, USA, 9 pages.

1 Introduction

Deep learning (DL) has achieved remarkable success in recent years, driven by advancements in computational resources and large-scale datasets [20]. With the rise of large language models, such as GPT-3, which has 175 billion parameters and was trained on 45 terabytes of text data using thousands of GPUs for a month [1], the demand for computational power and data has reached unprecedented levels. However, the exponential growth of data has created a significant imbalance with computational capacity, posing challenges to training efficiency and costs [18].

Dataset distillation (DD) has recently emerged as a promising solution to the challenges posed by large-scale datasets and their computational demands [9]. By synthesizing smaller datasets that retain the essential information of the raw data, DD enables efficient training while significantly reducing storage and computational costs, with minimal impact on model performance [28]. With advantages such as lower storage, training, and energy costs, DD is expected to become a widely adopted method for data sharing, playing a pivotal role in many machine learning applications [37].

Most existing DD methods focus solely on preserving the information of the raw dataset, often overlooking security issues. While these issues have recently garnered some attention from researchers, the number of related studies remains limited. For example, Liu *et al.* [23] proposed DoorPing, a learnable trigger that is iteratively updated during the distillation procedure. Similarly, Chung *et al.* [5] introduced a standard optimization framework to learn triggers for DD.

However, the threat models of these methods assume that the dataset owner intentionally injects backdoors during the distillation

*This work was conducted during the visiting tenure of Ziyuan Yang at the Agency for Science, Technology and Research (A*STAR).

[†]Corresponding Author

Permission to make digital or hard copies of all or part of this work for personal or classroom use is granted without fee provided that copies are not made or distributed for profit or commercial advantage and that copies bear this notice and the full citation on the first page. Copyrights for components of this work owned by others than the author(s) must be honored. Abstracting with credit is permitted. To copy otherwise, or republish, to post on servers or to redistribute to lists, requires prior specific permission and/or a fee. Request permissions from permissions@acm.org.
Conference'17, Washington, DC, USA

© 2018 Copyright held by the owner/author(s). Publication rights licensed to ACM.
ACM ISBN 978-x-xxxx-xxxx-x/YYYY/MM

¹The code will be made publicly available to ensure reproducibility.

process. In practice, dataset owners are unlikely to compromise their own data by injecting backdoors. Instead, a more plausible threat arises from third-party adversaries. For instance, during dataset distribution, attackers may intercept access to a benign distilled dataset, inject backdoors, and redistribute the compromised version to unsuspecting users, enabling malicious activities. Additionally, distilled datasets are often considered privacy-preserving [7], secure [23], and highly compact, making them suitable for storage on various Internet-of-Things (IoT) devices or clients in distributed learning paradigm [33, 41]. This widespread deployment increases the risk of unauthorized access, facilitating manipulation of the dataset by attackers. Once compromised, the backdoored distilled dataset can be redistributed to other users, thereby amplifying the threat. To highlight the distinction between previous threat models and ours, we provide an illustrative example in Figure 1.

In this work, we consider a practical threat model where malicious behavior originates from third parties during data sharing. Specifically, we attempt to directly inject backdoors into the distilled dataset while ensuring that the malicious behavior can still be triggered by real images. This represents a particularly difficult attack assumption for attackers, as it relies on the premise that the malicious third party does not have access to any raw data. Moreover, the significant gap between synthetic and real images presents an additional challenge.

To address these challenges and evaluate the vulnerabilities of distilled datasets, we propose a novel and the first backdoor attack method specifically designed for this threat model. Under our strict assumption, the attacker has no access to raw data. However, the fundamental paradigm of DD involves synthesizing small-scale datasets that retain the knowledge of the raw dataset. This implies that the distilled dataset inherently encapsulates the knowledge of the raw data. While it is almost impossible to reconstruct visually similar images to the raw data without any prior knowledge, the inherent properties of DL enable us to focus on the deep feature space. We only need to ensure that the reconstructed images in the latent feature space share a similar distribution with real images, which allows the trigger to be effectively activated in this space. Leveraging this paradigm, we aim to reconstruct conceptual archetypes for each class, derived from the knowledge embedded in the model trained on the benign distilled dataset, to serve as the foundation of our attack.

Next, we inject backdoors into these conceptual archetypes while ensuring that the modified distilled dataset retains the knowledge of the raw dataset. To achieve this, we propose a hybrid loss function that injects backdoor information into the malicious distilled dataset while preserving the original optimization trajectory. This approach bridges the gap between the distilled dataset and real images, ensuring that the backdoor can be reliably activated by real images while minimizing performance degradation for benign images.

Notably, our method directly injects backdoors into the distilled dataset without requiring prior knowledge of the DD method, raw data, or the downstream model. Extensive experiments demonstrate that our approach can successfully compromise the security of distilled datasets, regardless of the DD method, downstream model architecture, or training strategy. This finding challenges the prevailing belief that distilled datasets are inherently secure [23] and

reveals significant security vulnerabilities. Additionally, our attack method is highly lightweight, capable of synthesizing malicious distilled datasets within one minute in certain scenarios. The main contributions can be summarized as follows:

- We investigate a novel threat model for DD, where backdoors are directly injected into distilled datasets without requiring any raw data access. To the best of our knowledge, this is the first study to explore this threat in DD.
- We propose the first backdoor injection method for distilled datasets that reconstructs conceptual archetypes and injects backdoors while preserving the knowledge of the raw dataset.
- We design a hybrid loss to ensure the backdoor injection aligns with the original optimization trajectory, maintaining backdoor activation in real images while minimizing performance degradation on benign tasks.
- Extensive experiments across diverse datasets, DD methods, networks, and training strategies validate the generalizability of our method and expose DD vulnerabilities. Moreover, our attack is highly efficient, synthesizing malicious distilled datasets in under a minute in certain cases.

2 Related Works

Dataset Distillation. DD aims to condense the richness of large-scale datasets into compact small datasets that effectively preserve training performance [36]. Coreset selection [8] is an early-stage research in data-efficient learning. Most methods rely on heuristics to select representatives. Unlike this paradigm, DD [31] aims to learn how to synthesize a tiny dataset that trains models to perform comparably to those trained on the complete dataset. Wang *et al.* [31] first proposed a bi-level meta-learning approach, which optimizes a synthetic dataset so that neural networks trained on it achieve the lowest loss on the raw dataset.

Following this research, many researchers have focused on reducing the computational cost of the inner loop by introducing closed-form solutions, such as kernel ridge regression [4, 24, 34]. Zhao *et al.* [40] proposed an approach that makes parameters trained on condensed data approximate the target parameters, formulating a gradient matching objective that simplifies the DD process from a parameter perspective. In [38], the authors enhanced the process by incorporating Differentiable Siamese Augmentation (DSA), which enables effective data augmentation on synthetic data and results in the distillation of more informative images. Additionally, Du *et al.* [8] proposed a sequential DD method to extract the high-level features learned by the DNN in later epochs. By combining meta-learning and parameter matching, Cazenavette *et al.* [2] proposed Matching Training Trajectories (MTT) and achieved satisfactory performance. Besides, a recent work, TESLA [6], reduced GPU memory consumption and can be viewed as a memory-efficient version of MTT.

Backdoor Attack. Backdoor attacks introduce malicious behavior into the model without degrading its performance on the original task by poisoning the dataset. Gu *et al.* [11] introduced the backdoor threat in DL with BadNets, which injects visible triggers into randomly selected training samples and mislabels them as a specified target class. To enhance attack stealthiness, Chen *et*

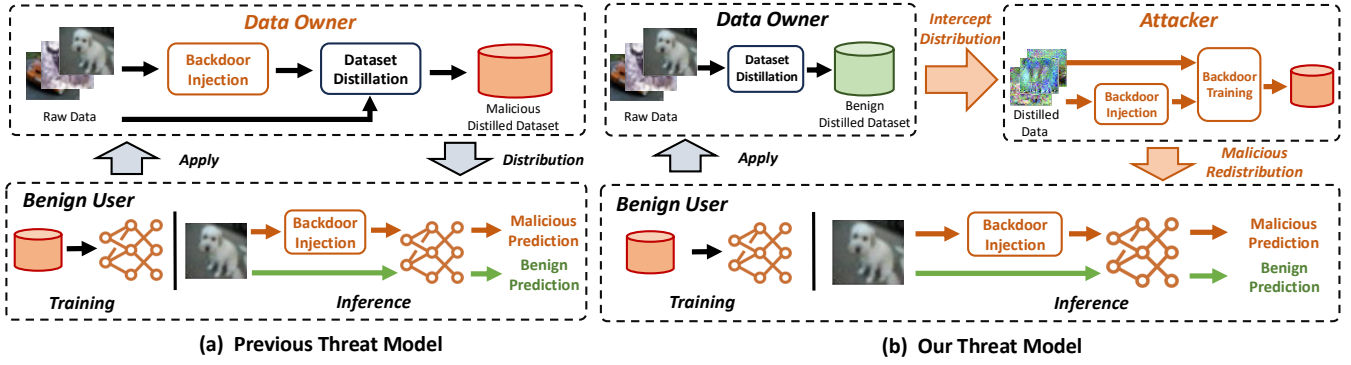


Figure 1: Illustration of the threat models. (a) Previous works assume that the data owner may be malicious and inject backdoors into the distilled dataset before distributing it to users. (b) In contrast, our threat model is more practical. We assume the data owner is benign. However, third parties, such as hackers or malicious users, may act maliciously. They could attack the system by hijacking the dataset distribution, injecting backdoors into the distilled dataset, and redistributing it to users.

al. [3] proposed a blended strategy to make poisoned images indistinguishable from benign ones, improving their ability to evade human inspection. Furthermore, subsequent works explored stealthier attacks: WaNet [26] used image warping; ISSBA [22] employed deep steganography; Feng *et al.* [10] and Wang *et al.* [30] embedded triggers in the frequency domain; Yang *et al.* [35] injected the trigger into the measurement domain; and Color Backdoor [13] utilized uniform color space shifts as triggers.

Although existing works have demonstrated the vulnerability of deep networks to backdoor attacks, the exploration of such vulnerabilities in the context of DD remains limited. Only a few studies have evaluated the security risks associated with DD [5, 23]. This highlights the urgent need for a deeper investigation into the potential threats and vulnerabilities specific to DD.

3 Threat Model

In previous works [5, 23], the threat model assumes all users are benign, the data owner is malicious, and the attack method has access to the raw data and knowledge of the specific DD method used. These are highly restrictive and unrealistic assumptions, as raw data and DD methods are typically strictly protected by the owner in practice. In contrast, our threat model adopts a more practical and relaxed assumption, not requiring all users to be benign and permitting the attacker to operate without access to the raw data.

Attack Scenario. In our threat model, the attacker intercepts the distribution process and injects backdoor information into the benign distilled dataset. The compromised dataset is then redistributed to users, allowing the attacker to manipulate the behavior of downstream models trained on the malicious dataset.

Attacker’s Goal. The primary goal of the attacker is to inject a backdoor into the distilled dataset, ensuring that downstream models trained on it exhibit malicious behavior when triggered, while maintaining high performance on benign inputs.

Attacker’s Capability. Our threat model imposes significant constraints on attackers. They do not have access to the raw dataset and can only interact with the distilled dataset, with no prior knowledge of the specific DD method used to generate it.

Challenges. *i) No Access to Raw Data:* The attacker has no access to the raw dataset and must infer meaningful information solely from the significantly smaller distilled dataset, often less than one percent of the raw dataset’s size. *ii) Bridging the Gap Between Synthetic and Real Images:* The distilled dataset is highly abstract and lacks the low-level visual details present in the raw data. The attacker must ensure that the injected backdoors are reliably triggered by real-world images in downstream tasks. *iii) Maintaining Dataset Utility:* The modified distilled dataset must remain effective for training models on legitimate tasks, ensuring the backdoor injection does not degrade overall performance.

4 Proposed Method

4.1 Problem Statement

As mentioned earlier, DD aims to extract knowledge from a large-scale dataset and construct a much smaller synthetic dataset, where models trained on it perform similarly to those trained on the raw dataset. Let \mathcal{T} denote the target dataset and \mathcal{S} the synthetic (distilled) dataset, where $|\mathcal{T}| \gg |\mathcal{S}|$, indicating that the distilled dataset is much smaller than the original. The loss between the prediction and ground truth is defined as ℓ . The DD process can then be formulated as [21]:

$$\mathbb{E}_{(x,y) \sim \mathcal{D}} [\ell(\mathcal{M}_{\mathcal{T}}(x), y)] \simeq \mathbb{E}_{(x,y) \sim \mathcal{D}} [\ell(\mathcal{M}_{\mathcal{S}}(x), y)], \quad (1)$$

where $\mathcal{M}_{\mathcal{T}}$ and $\mathcal{M}_{\mathcal{S}}$ denote the downstream model \mathcal{M} trained on \mathcal{T} and \mathcal{S} , respectively. \mathcal{D} denotes the real data distribution.

In this paper, we aim to update \mathcal{S} to obtain a malicious synthetic dataset $\hat{\mathcal{S}}$, which is injected with backdoor information. The goal is to ensure that malicious behavior is effectively triggered when a model is trained on $\hat{\mathcal{S}}$. The process can be formulated as:

$$\mathbb{E}_{x \sim \mathcal{D}} \left[\mathcal{M}_{\hat{\mathcal{S}}}(x + T) \right] \approx y_T, \quad (2)$$

where T is the trigger and y_T denotes the target label.

$$\alpha \mathcal{L}_{BA} + (1 - \alpha) \mathcal{L}_{tr}. \quad (3)$$

Furthermore, for benign samples, the performance gap between models trained on \mathcal{S} and $\hat{\mathcal{S}}$ should remain minimal to conceal the

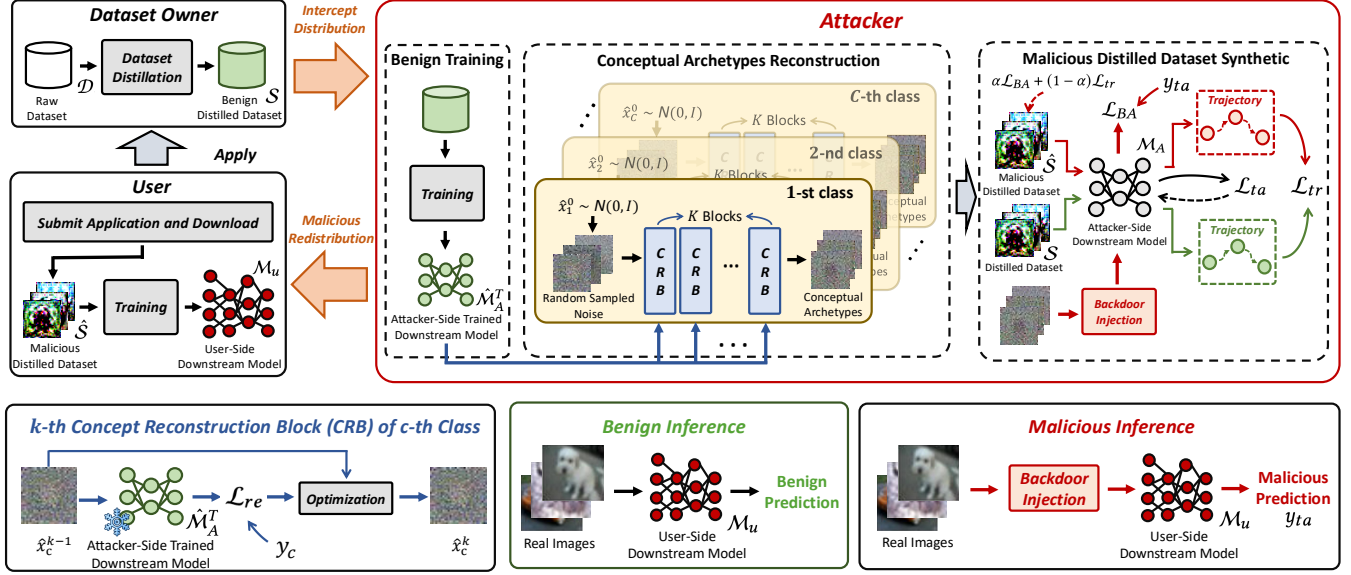


Figure 2: Overview of the proposed method.

malicious behavior. The problem can be formulated as:

$$\mathbb{E}_{(x,y) \sim \mathcal{D}} [\ell(\mathcal{M}_{\hat{S}}(x), y)] \approx \mathbb{E}_{(x,y) \sim \mathcal{D}} [\ell(\mathcal{M}_S(x), y)]. \quad (4)$$

4.2 Overview

The overview of the proposed method is illustrated in Figure 2. As described earlier, our threat model involves three entities: the dataset owner, the attacker, and the benign user. The dataset owner generates a benign distilled dataset \mathcal{S} from the raw dataset \mathcal{D} and distributes it to users upon request. The attacker intercepts the distribution process and converts the benign distilled dataset into a malicious version.

Specifically, our attack method consists of three main phases. First, the attacker trains a downstream model using the benign distilled dataset \mathcal{S} . Next, leveraging the trained model, the attacker reconstructs conceptual archetypes for each class using the proposed Concept Reconstruction Blocks (CRBs). Finally, the attacker injects backdoor information into reconstructed conceptual archetypes and employs a hybrid loss to update the distilled dataset, ensuring that the backdoor is embedded while minimizing performance degradation. Once the malicious distilled dataset is created, it is redistributed to users.

The benign user then trains the local model \mathcal{M}_u . Finally, the attacker can target the user-side system by injecting the triggers into real images, activating the malicious behavior in \mathcal{M}_u .

4.3 Proposed Attack Method

Our attack method consists of three main phases, which work together to effectively inject backdoor information while preserving the knowledge from the raw dataset. We detail each phase in the following sections:

Benign Training. After intercepting the distribution, the attacker first trains a benign downstream model using the distributed distilled dataset. The attacker-side trained downstream model is defined as $\hat{\mathcal{M}}_A^T$, which is the foundation of the subsequent phases.

Conceptual Archetypes Reconstruction. Under our strict assumption, the attacker has no access to real images and can only leverage the distilled dataset. However, during the inference phase, the system’s input typically consists of real images. This raises a critical question: *How can the backdoor be activated when injected into real images without relying on any raw data during backdoor training?*

To bridge the gap between distilled and real data, we propose reconstructing conceptual archetypes for each class. Although generating low-level, semantically similar images without access to raw data is infeasible, this limitation is not critical. In deep networks, accurate classification primarily relies on ensuring that the latent feature representations of the conceptual archetypes closely align with those of the real images.

The reconstruction process aims to generate conceptual archetypes for each class by iteratively refining random noise to align with the high-level feature representations of the target class in $\hat{\mathcal{M}}_A^T$. Specifically, for the c -th class, the process consists of K **Concept Reconstruction Blocks (CRBs)**, each corresponding to an optimization step. The conceptual archetype initialization process for each class c can be formulated as:

$$\hat{x}_c^0 \sim \mathcal{N}(0, I), \quad (5)$$

where $\mathcal{N}(0, I)$ represents a Gaussian distribution with zero mean and identity covariance matrix. $\hat{x}_c^0 \in \mathbb{R}^{C \times H \times W}$ denotes the initialized conceptual archetype for the c -th class, where C , H , and W denote the channel, height, and width of the distilled data, respectively.

In the k -th CRB block, \hat{x}_c^{k-1} is optimized to align the model’s output with the c -th class representation. The optimization objective

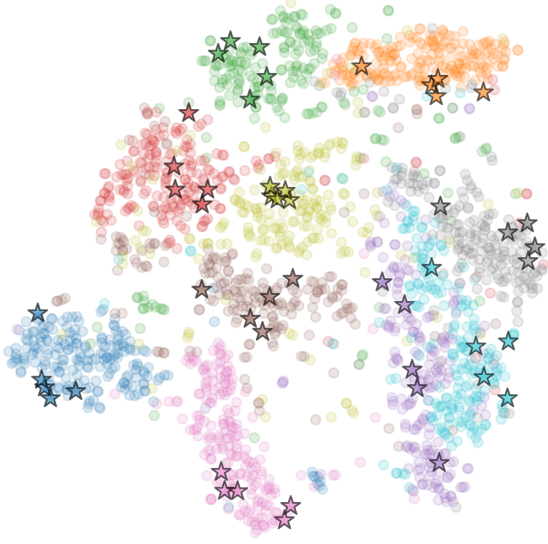


Figure 3: t-SNE visualization of the feature space. “Stars” and “Circles” represent the concept archetypes and real images, respectively. The reconstructed archetypes align closely with the deep feature representations of real images, effectively bridging the gap between the distilled data and real images.

is defined as follows:

$$\mathcal{L}_{re}(\hat{x}_c^{k-1}, c) = -y_c \log \left(\hat{M}_A^T(\hat{x}_c^{k-1})_c \right), \quad (6)$$

where \mathcal{L}_{re} is the reconstruction loss, y_c represents the one-hot encoded label for class c .

The optimization process can be formulated as:

$$\hat{x}_c^k = \hat{x}_c^{k-1} - \eta \cdot \nabla_{\hat{x}_c^{k-1}} \mathcal{L}_{re}(\hat{x}_c^{k-1}, c), \quad (7)$$

where η is the learning rate, and $\nabla_{\hat{x}_c^{k-1}} \mathcal{L}_{re}(\hat{x}_c^{k-1}, c)$ represents the gradient of the reconstruction loss with respect to the input \hat{x}_c^{k-1} .

After K iterations, the reconstructed image \hat{x}_c^K serves as the conceptual archetype for class c . This process is repeated m times for each class to generate m archetypes, with m set to 5 in this paper. Figure 3 illustrates a t-SNE visualization [29] comparing the deep feature representations of the conceptual archetypes with those of real images in MNIST [19]. The results show that the reconstructed archetypes closely align with the deep feature representations of real images, effectively bridging the gap between the distilled dataset and real images.

Malicious Distilled Dataset Synthesis. The goal of the attack is to synthesize a malicious distilled dataset such that the backdoor can be effectively activated by real images while maintaining the utility of the dataset for benign tasks. By reconstructing conceptual archetypes to bridge the gap between the distilled and real data, we can leverage them to embed malicious knowledge into the distilled dataset.

Specifically, for each conceptual archetype \hat{x} , we obtain the backdoored sample \hat{x}' as follows:

$$\hat{x}'(h, w) = \begin{cases} v, & \text{if } h \geq H - t \text{ and } w \geq W - t, \\ \hat{x}(h, w), & \text{otherwise,} \end{cases} \quad (8)$$

where v represents the trigger value and t specifies the trigger size.

Then, a backdoor loss is designed to embed malicious information into the distilled dataset, ensuring that the backdoor behavior is learned by the model trained on the modified data. The backdoor loss is defined as:

$$\mathcal{L}_{BA} = -y_{ta} \log \left(\mathcal{M}_A(\hat{x}')_{ta} \right), \quad (9)$$

where y_{ta} represents the backdoor target label, and \mathcal{M}_A is the attacker-side model, trained from scratch.

To conceal the malicious behavior from detection, it is essential to minimize performance degradation. This requires ensuring that the optimization trajectory of downstream models trained on the malicious distilled dataset closely aligns with those trained on the benign distilled dataset. Specifically, a trajectory consistency loss is introduced to enforce this alignment as follows:

$$\mathcal{L}_{tr} = \frac{1}{|\Theta|} \sum_{\theta \in \Theta} \|\nabla_{\theta} \mathcal{L}_{ta}(\mathcal{S}) - \nabla_{\theta} \mathcal{L}_{ta}(\hat{\mathcal{S}})\|^2, \quad (10)$$

where Θ denotes the set of model parameters of \mathcal{M}_A , \mathcal{L}_{ta} represents the loss of the downstream task.

By constraining \mathcal{L}_{tr} , we can ensure that the malicious dataset maintains a similar optimization trajectory to the benign dataset, thereby concealing malicious behavior while minimizing the impact on the performance of downstream tasks. Finally, we combine both losses to form the overall objective for synthesizing the malicious distilled dataset. The hybrid loss function is defined as follows:

$$\mathcal{L}_{hybrid} = \alpha \mathcal{L}_{BA} + (1 - \alpha) \mathcal{L}_{tr}, \quad (11)$$

where α is the balancing parameter that controls the trade-off between embedding malicious information and maintaining trajectory consistency.

Then, $\hat{\mathcal{S}}$ is iteratively updated to minimize \mathcal{L}_{hybrid} as:

$$\hat{\mathcal{S}} \leftarrow \hat{\mathcal{S}} - \eta \cdot \nabla \mathcal{L}_{hybrid}. \quad (12)$$

These steps are repeated for N iterations within a single epoch. To ensure that model \mathcal{M}_A follows the next benign optimization trajectory, it is updated on \mathcal{S} after each epoch. This entire process is repeated for E epochs.

Implementation. Once the attacker synthesizes the malicious distilled dataset $\hat{\mathcal{S}}$, it is redistributed to the users. Users then train their downstream models \mathcal{M}_u on $\hat{\mathcal{S}}$ using their own training strategies.

During the inference phase, the malicious behavior is activated when the trigger is injected into real images following Eq. (8) to produce malicious outputs aligned with the attacker’s target, while maintaining normal performance on benign inputs.

Notably, our attack method remains effective even when \mathcal{M}_u and \mathcal{M}_A have different architectures. Furthermore, it does not require fine-tuning any DD process on the dataset owner’s side, nor does it require access to raw data. Therefore, our method is versatile and practical across various scenarios.

5 Experiments

5.1 Experimental Setting

Experiment Environment. Our proposed method is implemented using the PyTorch framework and optimized with Stochastic Gradient Descent (SGD) [14] with a learning rate of 0.01. The number of epochs for synthesizing the malicious dataset is set to 10. The

Table 1: Experimental results of different strategies and different raw datasets with DC (Avg \pm STD, %).

	IPC	Epoch Metric	Epoch									
			10	20	30	40	50	60	70	80	90	100
CIFAR10	1	Baseline	26.88 \pm 0.405	27.25 \pm 0.500	27.56 \pm 0.481	27.85 \pm 0.428	27.78 \pm 0.592	27.85 \pm 0.526	27.83 \pm 0.631	27.45 \pm 0.607	27.52 \pm 0.753	27.77 \pm 0.383
		BA	25.07 \pm 0.475	25.47 \pm 0.610	25.42 \pm 0.574	25.50 \pm 0.579	25.43 \pm 0.415	25.82 \pm 0.649	25.31 \pm 0.611	25.71 \pm 0.508	25.32 \pm 0.521	25.79 \pm 0.448
		ASR	99.82 \pm 0.150	99.99 \pm 0.009	100.00 \pm 0.000	99.99 \pm 0.013	100.00 \pm 0.006	100.00 \pm 0.000	100.00 \pm 0.000	100.00 \pm 0.003	100.00 \pm 0.006	100.00 \pm 0.003
	10	Baseline	26.57 \pm 0.996	31.85 \pm 0.836	35.62 \pm 0.466	38.40 \pm 0.447	39.93 \pm 0.760	40.86 \pm 0.484	41.49 \pm 0.620	41.99 \pm 0.441	42.77 \pm 0.745	42.63 \pm 0.426
		BA	25.82 \pm 0.749	30.22 \pm 0.611	32.59 \pm 0.540	34.07 \pm 0.391	34.87 \pm 0.386	35.24 \pm 0.417	35.32 \pm 0.585	35.98 \pm 0.491	35.60 \pm 0.376	35.92 \pm 0.442
		ASR	99.99 \pm 0.008	100.00 \pm 0.000	100.00 \pm 0.000	100.00 \pm 0.000	100.00 \pm 0.000	100.00 \pm 0.000	99.99 \pm 0.013	100.00 \pm 0.009	100.00 \pm 0.012	100.00 \pm 0.003
CIFAR100	1	Baseline	3.36 \pm 0.270	6.13 \pm 0.264	7.99 \pm 0.548	9.05 \pm 0.471	9.46 \pm 0.294	10.22 \pm 0.380	10.52 \pm 0.237	10.69 \pm 0.335	11.11 \pm 0.318	10.77 \pm 0.294
		BA	3.05 \pm 0.338	5.95 \pm 0.319	7.24 \pm 0.317	8.36 \pm 0.418	8.59 \pm 0.138	9.19 \pm 0.190	9.39 \pm 0.220	9.75 \pm 0.204	9.81 \pm 0.268	9.97 \pm 0.374
		ASR	22.56 \pm 27.631	87.38 \pm 10.855	96.93 \pm 6.836	98.89 \pm 0.849	99.26 \pm 1.155	99.80 \pm 0.285	99.49 \pm 0.730	99.85 \pm 0.160	99.57 \pm 0.600	99.83 \pm 0.153
	10	Baseline	70.69 \pm 2.768	79.73 \pm 2.424	82.19 \pm 0.874	84.91 \pm 1.659	85.92 \pm 0.944	86.38 \pm 1.227	86.75 \pm 0.730	87.27 \pm 0.737	87.89 \pm 0.553	88.81 \pm 0.867
		BA	65.69 \pm 2.740	70.42 \pm 2.298	73.91 \pm 2.185	75.04 \pm 2.094	76.65 \pm 1.384	77.00 \pm 1.612	77.55 \pm 1.518	78.38 \pm 1.458	78.75 \pm 1.235	79.45 \pm 1.073
		ASR	100.00 \pm 0.000	100.00 \pm 0.000	100.00 \pm 0.000	100.00 \pm 0.000	100.00 \pm 0.000	100.00 \pm 0.000	100.00 \pm 0.000	100.00 \pm 0.000	100.00 \pm 0.000	100.00 \pm 0.000
50	Baseline	69.75 \pm 5.173	80.26 \pm 2.411	83.67 \pm 0.885	86.17 \pm 0.703	89.32 \pm 0.510	91.49 \pm 0.471	93.23 \pm 0.246	94.63 \pm 0.287	95.17 \pm 0.170	95.72 \pm 0.232	
	BA	63.76 \pm 3.923	75.31 \pm 1.948	79.98 \pm 1.134	82.05 \pm 1.565	85.09 \pm 1.058	87.51 \pm 0.817	89.35 \pm 0.661	90.07 \pm 0.458	90.39 \pm 1.048	90.41 \pm 0.478	
	ASR	100.00 \pm 0.000	100.00 \pm 0.000	100.00 \pm 0.000	100.00 \pm 0.000	100.00 \pm 0.000	100.00 \pm 0.000	100.00 \pm 0.000	100.00 \pm 0.000	100.00 \pm 0.000	100.00 \pm 0.000	
MNIST	1	Baseline	78.09 \pm 1.537	85.41 \pm 0.717	90.01 \pm 0.653	93.57 \pm 0.293	95.09 \pm 0.154	95.98 \pm 0.189	96.69 \pm 0.110	97.13 \pm 0.140	97.44 \pm 0.111	97.74 \pm 0.072
		BA	64.23 \pm 4.176	68.67 \pm 1.887	74.48 \pm 1.117	79.52 \pm 1.135	85.17 \pm 1.045	87.25 \pm 0.670	88.49 \pm 0.663	88.94 \pm 0.540	89.32 \pm 0.466	89.31 \pm 0.625
		ASR	100.00 \pm 0.000	100.00 \pm 0.000	100.00 \pm 0.000	100.00 \pm 0.000	100.00 \pm 0.000	100.00 \pm 0.000	100.00 \pm 0.000	100.00 \pm 0.000	100.00 \pm 0.000	100.00 \pm 0.000
	10	Baseline	67.51 \pm 0.399	69.29 \pm 0.741	69.45 \pm 0.908	69.81 \pm 0.843	69.88 \pm 0.715	70.10 \pm 0.787	69.94 \pm 0.553	69.86 \pm 0.553	69.84 \pm 0.525	69.98 \pm 0.680
		BA	61.75 \pm 1.044	63.29 \pm 0.741	63.72 \pm 0.803	63.66 \pm 0.870	63.66 \pm 0.382	63.70 \pm 0.661	63.37 \pm 0.755	63.93 \pm 0.933	63.94 \pm 0.786	63.93 \pm 0.553
		ASR	100.00 \pm 0.000	100.00 \pm 0.000	100.00 \pm 0.000	100.00 \pm 0.000	100.00 \pm 0.000	100.00 \pm 0.000	100.00 \pm 0.000	100.00 \pm 0.000	100.00 \pm 0.000	100.00 \pm 0.000
50	Baseline	60.92 \pm 1.977	66.27 \pm 1.095	69.41 \pm 0.766	72.39 \pm 0.445	74.29 \pm 0.468	75.51 \pm 0.296	76.41 \pm 0.278	77.61 \pm 0.393	78.15 \pm 0.176	78.81 \pm 0.209	
	BA	59.84 \pm 4.410	65.94 \pm 1.568	69.02 \pm 1.264	69.83 \pm 0.799	71.02 \pm 0.561	71.12 \pm 0.482	70.89 \pm 0.744	71.36 \pm 0.738	71.17 \pm 0.533	71.42 \pm 0.633	
	ASR	100.00 \pm 0.000	100.00 \pm 0.000	100.00 \pm 0.000	100.00 \pm 0.000	100.00 \pm 0.000	100.00 \pm 0.000	100.00 \pm 0.000	100.00 \pm 0.000	100.00 \pm 0.000	100.00 \pm 0.000	
FashionMNIST	1	Baseline	65.95 \pm 0.638	69.32 \pm 0.390	71.54 \pm 0.273	72.94 \pm 0.279	74.73 \pm 0.289	76.17 \pm 0.273	77.16 \pm 0.325	77.85 \pm 0.213	78.71 \pm 0.253	79.40 \pm 0.148
		BA	63.04 \pm 0.868	67.18 \pm 0.499	69.22 \pm 0.260	69.95 \pm 0.454	69.96 \pm 0.268	70.01 \pm 0.350	69.32 \pm 0.347	69.58 \pm 0.447	69.37 \pm 0.353	69.49 \pm 0.704
		ASR	100.00 \pm 0.000	100.00 \pm 0.000	100.00 \pm 0.000	100.00 \pm 0.000	100.00 \pm 0.000	99.94 \pm 0.089	99.93 \pm 0.059	99.64 \pm 0.434	99.58 \pm 0.434	99.51 \pm 0.461
	10	Baseline	29.10 \pm 1.480	31.58 \pm 1.154	31.37 \pm 1.511	30.63 \pm 1.027	29.91 \pm 0.851	29.90 \pm 0.977	30.51 \pm 1.481	29.47 \pm 0.898	30.20 \pm 1.023	30.64 \pm 1.842
		BA	29.30 \pm 1.276	30.59 \pm 0.979	29.70 \pm 1.376	29.05 \pm 1.842	28.69 \pm 1.322	29.57 \pm 1.004	28.88 \pm 1.080	28.99 \pm 1.718	29.56 \pm 0.957	29.47 \pm 0.926
		ASR	100.00 \pm 0.000	100.00 \pm 0.000	100.00 \pm 0.000	100.00 \pm 0.000	100.00 \pm 0.000	100.00 \pm 0.000	100.00 \pm 0.000	100.00 \pm 0.000	100.00 \pm 0.000	100.00 \pm 0.000
50	Baseline	29.10 \pm 1.480	31.58 \pm 1.154	31.37 \pm 1.511	30.63 \pm 1.027	29.91 \pm 0.851	29.90 \pm 0.977	30.51 \pm 1.481	29.47 \pm 0.898	30.20 \pm 1.023	30.64 \pm 1.842	
	BA	29.30 \pm 1.276	30.59 \pm 0.979	29.70 \pm 1.376	29.05 \pm 1.842	28.69 \pm 1.322	29.57 \pm 1.004	28.88 \pm 1.080	28.99 \pm 1.718	29.56 \pm 0.957	29.47 \pm 0.926	
	ASR	100.00 \pm 0.000	100.00 \pm 0.000	100.00 \pm 0.000	100.00 \pm 0.000	100.00 \pm 0.000	100.00 \pm 0.000	100.00 \pm 0.000	100.00 \pm 0.000	100.00 \pm 0.000	100.00 \pm 0.000	
SVHN	1	Baseline	29.10 \pm 1.480	31.58 \pm 1.154	31.37 \pm 1.511	30.63 \pm 1.027	29.91 \pm 0.851	29.90 \pm 0.977	30.51 \pm 1.481	29.47 \pm 0.898	30.20 \pm 1.023	30.64 \pm 1.842
		BA	29.30 \pm 1.276	30.59 \pm 0.979	29.70 \pm 1.376	29.05 \pm 1.842	28.69 \pm 1.322	29.57 \pm 1.004	28.88 \pm 1.080	28.99 \pm 1.718	29.56 \pm 0.957	29.47 \pm 0.926
		ASR	100.00 \pm 0.000	100.00 \pm 0.000	100.00 \pm 0.000	100.00 \pm 0.000	100.00 \pm 0.000	100.00 \pm 0.000	100.00 \pm 0.000	100.00 \pm 0.000	100.00 \pm 0.000	100.00 \pm 0.000

experiments are conducted on a system with an AMD Ryzen 7 5800X CPU @3.80 GHz, 32 GB of RAM, and an NVIDIA GTX 3090.

Experiment Setting. In our experiments, we use ConvNet [16] as the default attacker-side downstream model. Additionally, AlexNet [17], VGG11 [27], VGG16 [27], ResNet18 [12], and ResNet34 [12] are used as the user-side downstream networks.

Datasets. To assess the generalization ability of our method across different raw datasets, we evaluate it on CIFAR-10 [15], CIFAR-100 [15], MNIST [19], FashionMNIST [32], and SVHN [25].

DD Methods. To evaluate the generalizability of our method, we test it across several different representative DD methods, including DC [40], DM [39], DSA [38], and MTT [2].

Metrics. Similar to other backdoor attack methods [11], we adopt benign accuracy (BA) to measure performance on benign samples. Besides, we use attack success rate (ASR) to the effectiveness of our attack.

Neural networks exhibit inherent randomness due to variations introduced by different random seeds. To ensure the reliability of our results, we conduct experiments with 10 different seeds and report both the average (Avg) and standard deviation (STD) of the performance metrics.

5.2 Experiments about Different Training Strategies

In this subsection, we evaluate the impact of different training strategies on the effectiveness of our attack based on DC. Specifically, we analyze performance across different numbers of training epochs in user-side training, and we treat the performance of models trained directly on the benign distilled dataset as the baseline.

As shown in Table 1, our attack remains highly effective across different numbers of training epochs, consistently maintaining a high ASR while inducing minimal BA degradation. Besides, our method demonstrates strong generalizability across various raw datasets and different images per class (IPC) settings, ensuring its robustness in diverse scenarios.

In previous experiments, we assume that the user-side model was identical to the attacker’s model. To further validate the robustness of our method, we investigate a more challenging scenario where the user-side model differs from the attacker’s model. We analyze the attack performance under different training strategies, and the results are presented in Figure 4. In this experiment, we use CIFAR-10 as the raw dataset based on DC with setting IPC to 1. As shown in the results, our method remains highly effective, consistently delivering strong attack performance even when the user-side model differs from the attacker’s model.

5.3 Experiment with Different Dataset Distillation Methods

To further validate the effectiveness of our attack, we extend our experiments to different DD methods, with the results summarized in Table 2. We conduct evaluations using user-side training strategies of 50 and 100 epochs. As shown in Table 2, our attack consistently demonstrates strong performance across various DD methods. In most cases, the attack achieves nearly 100% ASR, effectively embedding the backdoor into the distilled dataset, regardless of the specific DD approach employed. Additionally, the BA degradation remains within an acceptable range, which indicates that the overall utility of the dataset is well preserved. These results

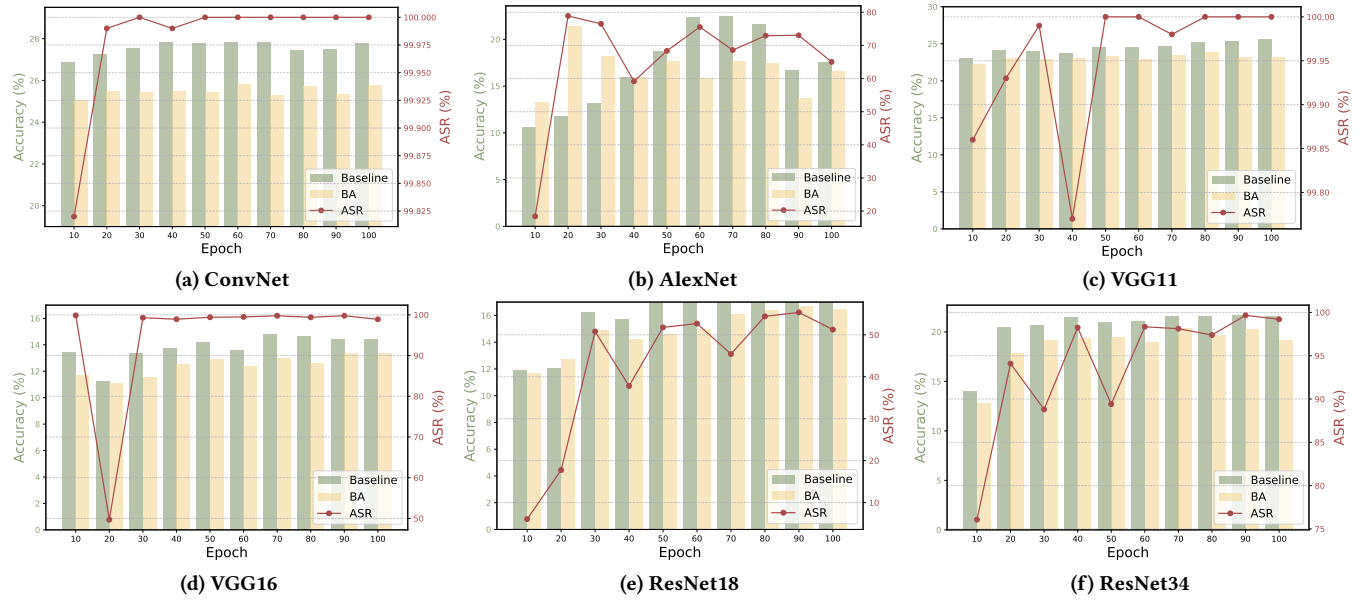


Figure 4: The performances of different user-side models under different training strategies. Our attack consistently poses a significant threat across different user-side models and training strategies.

Table 2: Experimental results based on different DD methods and different user-side models (Avg \pm STD, %).

Method	Dataset	IPC	ConvNet		AlexNet		VGG11		VGG16		ResNet18		ResNet34		
			50	100	50	100	50	100	50	100	50	100	50	100	
DC	CIFAR10	1	Baseline	27.78 \pm 0.592	27.77 \pm 0.383	18.77 \pm 0.022	17.56 \pm 0.275	24.47 \pm 0.921	25.66 \pm 0.952	14.16 \pm 1.069	14.42 \pm 0.958	16.96 \pm 1.073	17.93 \pm 1.021	21.01 \pm 0.886	21.58 \pm 0.851
			BA	25.43 \pm 0.415	25.79 \pm 0.448	17.68 \pm 2.401	16.57 \pm 3.968	23.24 \pm 0.747	23.17 \pm 0.921	12.90 \pm 0.866	13.37 \pm 1.015	14.62 \pm 1.645	16.49 \pm 0.970	19.45 \pm 1.062	19.17 \pm 1.404
			ASR	100.00 \pm 0.006	100.00 \pm 0.003	68.35 \pm 30.250	65.03 \pm 33.621	100.00 \pm 0.010	100.00 \pm 0.004	99.40 \pm 1.310	98.90 \pm 2.106	51.77 \pm 39.082	51.24 \pm 26.014	89.41 \pm 18.270	99.21 \pm 1.374
		10	Baseline	39.93 \pm 0.760	42.63 \pm 0.426	12.79 \pm 1.573	21.48 \pm 0.729	34.67 \pm 0.618	35.27 \pm 0.497	23.71 \pm 1.556	26.16 \pm 1.630	17.20 \pm 1.152	18.52 \pm 1.199	22.08 \pm 1.464	22.88 \pm 1.339
			BA	34.877 \pm 0.386	35.927 \pm 0.442	22.26 \pm 4.296	16.38 \pm 4.778	28.48 \pm 0.571	29.07 \pm 0.903	20.76 \pm 0.722	22.15 \pm 0.876	14.02 \pm 0.665	14.25 \pm 0.746	17.73 \pm 0.830	18.47 \pm 0.951
			ASR	100.00 \pm 0.000	100.00 \pm 0.003	96.84 \pm 6.607	41.41 \pm 41.240	100.00 \pm 0.000	100.00 \pm 0.000	100.00 \pm 0.000	100.00 \pm 0.000	75.51 \pm 17.345	88.00 \pm 14.494	99.95 \pm 0.131	99.97 \pm 0.096
	FashionMNIST	1	Baseline	9.46 \pm 0.294	10.77 \pm 0.294	2.11 \pm 0.197	1.68 \pm 0.520	8.41 \pm 0.356	9.01 \pm 0.208	3.15 \pm 0.436	4.61 \pm 0.599	1.53 \pm 0.140	1.67 \pm 0.184	2.26 \pm 0.214	3.16 \pm 0.461
			BA	8.59 \pm 0.138	9.97 \pm 0.374	2.11 \pm 0.319	1.33 \pm 0.401	7.06 \pm 0.334	7.85 \pm 0.295	2.85 \pm 0.742	4.09 \pm 0.389	1.34 \pm 0.146	1.39 \pm 0.166	1.71 \pm 0.131	2.30 \pm 0.229
			ASR	99.26 \pm 1.155	99.83 \pm 0.153	33.27 \pm 27.747	0.00 \pm 0.000	97.67 \pm 3.981	99.17 \pm 2.364	91.98 \pm 23.926	87.85 \pm 24.757	0.40 \pm 0.544	0.03 \pm 0.066	22.94 \pm 23.976	15.05 \pm 22.299
		10	Baseline	69.88 \pm 0.715	69.98 \pm 0.680	52.15 \pm 4.806	30.74 \pm 14.513	59.75 \pm 4.468	62.72 \pm 2.498	23.80 \pm 5.390	31.16 \pm 5.491	57.98 \pm 1.642	57.29 \pm 1.721	61.80 \pm 1.846	61.92 \pm 1.641
			BA	63.66 \pm 0.382	63.93 \pm 0.553	29.17 \pm 16.787	20.30 \pm 14.193	55.05 \pm 2.035	55.46 \pm 3.141	21.60 \pm 4.460	27.60 \pm 3.811	50.18 \pm 1.812	51.59 \pm 1.355	54.87 \pm 2.604	53.47 \pm 3.275
			ASR	100.00 \pm 0.000	100.00 \pm 0.000	74.46 \pm 40.198	68.27 \pm 41.138	100.00 \pm 0.000	100.00 \pm 0.000	100.00 \pm 0.000	100.00 \pm 0.000	99.66 \pm 0.646	98.43 \pm 4.697	100.00 \pm 0.000	100.00 \pm 0.000
DM	CIFAR10	50	Baseline	48.50 \pm 0.470	54.19 \pm 0.405	20.23 \pm 4.414	35.50 \pm 1.040	42.50 \pm 0.604	42.97 \pm 0.590	28.18 \pm 1.521	29.88 \pm 1.151	25.77 \pm 0.577	26.11 \pm 0.881	26.36 \pm 0.830	27.79 \pm 0.654
			BA	33.42 \pm 0.688	35.26 \pm 0.620	20.39 \pm 5.763	23.99 \pm 5.312	29.00 \pm 0.666	29.45 \pm 0.695	18.35 \pm 0.629	20.23 \pm 1.523	15.92 \pm 0.691	16.04 \pm 0.541	17.92 \pm 0.868	18.49 \pm 0.726
			ASR	99.91 \pm 0.108	99.25 \pm 0.406	84.05 \pm 30.952	97.89 \pm 3.954	100.00 \pm 0.000	100.00 \pm 0.000	100.00 \pm 0.000	100.00 \pm 0.000	99.88 \pm 0.306	98.93 \pm 1.866	100.00 \pm 0.000	100.00 \pm 0.000
		100	Baseline	26.24 \pm 0.566	26.69 \pm 0.807	19.25 \pm 1.465	17.04 \pm 2.166	21.99 \pm 0.714	22.23 \pm 1.054	13.53 \pm 0.867	15.07 \pm 0.752	23.49 \pm 1.063	25.00 \pm 0.957	21.18 \pm 1.138	22.06 \pm 1.179
			BA	24.09 \pm 0.719	24.70 \pm 0.552	18.65 \pm 1.322	16.50 \pm 3.057	19.01 \pm 1.579	21.60 \pm 1.066	12.24 \pm 1.515	13.12 \pm 0.840	20.89 \pm 0.806	22.48 \pm 0.433	18.24 \pm 1.034	19.38 \pm 1.397
			ASR	100.00 \pm 0.004	99.99 \pm 0.029	68.90 \pm 34.971	67.72 \pm 33.232	97.38 \pm 5.153	99.76 \pm 0.714	89.64 \pm 29.715	90.52 \pm 26.595	96.27 \pm 6.907	99.83 \pm 0.216	89.81 \pm 18.501	97.34 \pm 5.506
DSA	CIFAR100	1	Baseline	38.17 \pm 0.600	44.23 \pm 0.549	14.48 \pm 2.514	27.51 \pm 0.830	33.25 \pm 0.905	37.30 \pm 1.589	19.60 \pm 2.356	24.15 \pm 1.801	24.53 \pm 0.715	29.56 \pm 0.585	21.10 \pm 1.343	25.50 \pm 2.116
			BA	32.60 \pm 0.672	34.82 \pm 0.449	17.92 \pm 5.770	22.32 \pm 2.974	26.54 \pm 1.061	31.21 \pm 1.015	17.80 \pm 1.006	19.15 \pm 1.476	19.62 \pm 1.298	23.82 \pm 0.696	18.70 \pm 0.939	20.40 \pm 2.199
			ASR	100.00 \pm 0.000	100.00 \pm 0.000	46.18 \pm 43.370	47.10 \pm 33.155	100.00 \pm 0.000	100.00 \pm 0.000	99.99 \pm 0.042	100.00 \pm 0.000	98.22 \pm 5.314	100.00 \pm 0.006	99.34 \pm 1.842	100.00 \pm 0.003
		10	Baseline	8.78 \pm 0.402	9.99 \pm 0.461	1.24 \pm 0.145	2.55 \pm 0.649	6.15 \pm 0.205	8.27 \pm 0.579	2.07 \pm 0.263	3.11 \pm 0.686	2.94 \pm 0.228	5.63 \pm 0.334	3.31 \pm 0.231	5.15 \pm 0.507
			BA	7.66 \pm 0.262	9.10 \pm 0.242	2.41 \pm 0.524	1.97 \pm 1.109	5.79 \pm 0.509	7.35 \pm 0.468	2.23 \pm 0.234	3.05 \pm 0.466	2.20 \pm 0.288	4.07 \pm 0.523	3.14 \pm 0.356	4.27 \pm 0.499
			ASR	95.31 \pm 5.524	98.43 \pm 1.799	19.75 \pm 24.239	1.21 \pm 2.263	90.56 \pm 20.012	99.69 \pm 0.595	82.52 \pm 28.957	98.61 \pm 3.621	16.68 \pm 17.132	79.71 \pm 20.856	84.15 \pm 24.500	82.86 \pm 28.564
	FashionMNIST	1	Baseline	16.28 \pm 0.365	23.28 \pm 0.364	5.84 \pm 0.848	14.69 \pm 0.601	11.79 \pm 0.466	17.81 \pm 0.484	4.43 \pm 0.418	7.17 \pm 0.520	6.15 \pm 0.416	7.83 \pm 0.476	5.58 \pm 0.509	7.61 \pm 0.524
			BA	7.31 \pm 0.180	8.35 \pm 0.133	7.14 \pm 1.610	6.89 \pm 2.915	7.23 \pm 0.214	8.23 \pm 0.171	3.18 \pm 0.415	4.87 \pm 0.509	3.85 \pm 0.375	4.96 \pm 0.339	3.53 \pm 0.441	4.83 \pm 0.351
			ASR	42.76 \pm 9.156	41.90 \pm 6.128	35.68 \pm 7.267	25.76 \pm 27.264	96.23 \pm 2.352	60.21 \pm 11.040	97.17 \pm 5.463	75.47 \pm 17.501	95.90 \pm 2.960	75.79 \pm 13.136	98.16 \pm 1.720	67.59 \pm 8.190
		10	Baseline	67.89 \pm 1.046	69.22 \pm 0.821	42.81 \pm 4.420	45.75 \pm 15.920	53.03 \pm 3.175	57.14 \pm 2.398	21.53 \pm 3.859	27.98 \pm 5.190	62.66 \pm 1.644	66.32 \pm 1.923	57.96 \pm 2.942	58.88 \pm 1.684
			BA	61.32 \pm 1.001	62.55 \pm 1.303	32.27 \pm 13.479	32.55 \pm 15.653	47.77 \pm 1.926	49.78 \pm 1.856	19.57 \pm 3.460	28.21 \pm 6.489	56.31 \pm 0.988	57.36 \pm 2.118	49.29 \pm 3.731	50.07 \pm 3.197
			ASR	100.00 \pm 0.000	100.00 \pm 0.000	83.07 \pm 29.260	67.64 \pm 40.277	100.00 \pm 0.000	100.00 \pm 0.000	100.00 \pm 0.000	100.00 \pm 0.000	100.00 \pm 0.000	100.00 \pm 0.000	100.00 \pm 0.000	100.00 \pm 0.000
MTT	CIFAR10	1	Baseline	38.76 \pm 1.091	38.80 \pm 1.235	10.87 \pm 1.084	14.16 \pm 3.897	17.97 \pm 1.501	21.49 \pm 1.605	11.37 \pm 1.230	11.04 \pm 0.639	14.02 \pm 0.912	14.79 \pm 0.698	16.76 \pm 0.992	16.99 \pm 1.019
			BA	31.87 \pm 1.087	32.58 \pm 0.841	11.27 \pm 2.660	12.27 \pm 3.573	18.11 \pm 1.473	19.73 \pm 1.180	10.62 \pm 0.641	11.52 \pm 0.930	12.29 \pm 1.076	13.82 \pm 1.125	16.28 \pm 1.209	16.45 \pm 0.811
			ASR	100.00 \pm 0.000	100.00 \pm 0.000	70.29 \pm 45.392	72.69 \pm 37.554	100.00 \pm 0.000	100.00 \pm 0.000	100.00 \pm 0.000	98.89 \pm 2.271	59.24 \pm 36.482	92.44 \pm 10.594	99.94 \pm 0.123	99.64 \pm 1.068
		10	Baseline	43.81 \pm 0.709	51.65 \pm 0.926	16.82 \pm 3.091	26.73 \pm 1.160	33.44 \pm 0.593	34.35 \pm 1.110	23.33 \pm 2.895	25.66 \pm 1.848	15.58 \pm 0.367	16.17 \pm 0.829	19.53 \pm 1.148	21.22 \pm 0.675
			BA	34.81 \pm 0.436	37.81 \pm 0.569	24.13 \pm 4.853	11.66 \pm 2.302	25.00 \pm 1.176	25.92 \pm 1.154	17.01 \pm 1.617	20.44 \pm 1.647	12.33 \pm 0.309	12.74 \pm 0.672	14.73 \pm 0.831	16.06 \pm 1.442
			ASR	100.00 \pm 0.000	100.00 \pm 0.000	94.08 \pm 5.960	54.31 \pm 43.090	100.00 \pm 0.000	100.00 \pm 0.000	100.00 \pm 0.000	100.00 \pm 0.000	79.19 \pm 13.521	71.56 \pm 31.169	100.00 \pm 0.000	100.00 \pm 0.000

confirm the generalizability and robustness of our proposed attack method, demonstrating its effectiveness across different distillation strategies while maintaining the performance of downstream tasks.

5.4 Visualization

Figure 5 presents a visual comparison between benign and malicious distilled datasets. The first row displays examples of benign distilled images, while the second row illustrates their malicious

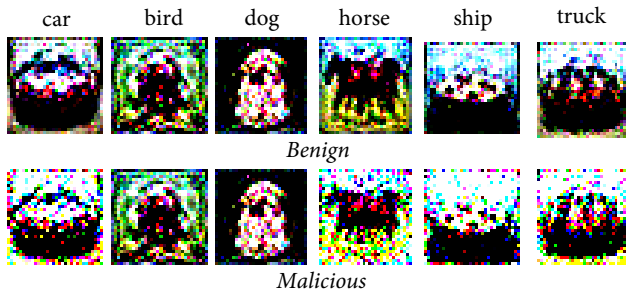


Figure 5: Visualization of benign and malicious distilled data. Without a direct comparison, users may struggle to sense the subtle differences due to the inherent abstraction of distilled datasets.

Table 3: Attack performance with different attacker-side downstream models (Avg \pm STD, %).

Model		DC	DSA	MTT
AlexNet	Baseline	21.48 \pm 0.729	27.51 \pm 0.830	26.73 \pm 1.160
	BA	16.56 \pm 6.264	21.65 \pm 1.919	19.86 \pm 3.226
	ASR	23.04 \pm 38.896	21.36 \pm 16.998	18.33 \pm 18.708
VGG11	Baseline	25.66 \pm 0.952	35.27 \pm 0.497	34.35 \pm 1.110
	BA	23.58 \pm 0.991	29.01 \pm 1.107	20.54 \pm 1.054
	ASR	68.89 \pm 20.244	49.77 \pm 26.597	77.21 \pm 20.196
VGG16	Baseline	26.16 \pm 1.630	24.15 \pm 1.801	25.66 \pm 1.848
	BA	21.01 \pm 2.285	21.69 \pm 1.418	21.57 \pm 1.493
	ASR	56.70 \pm 37.613	17.99 \pm 24.918	73.78 \pm 35.649

counterparts after backdoor injection. Due to the inherent abstraction of distilled datasets, these images inherently lack fine-grained details, making it challenging for users to discern their authenticity based on individual distilled samples. This abstraction further facilitates the attack, as the malicious modifications remain visually subtle and difficult to detect. Despite these seemingly minor perturbations, the backdoor triggers embedded in the malicious dataset remain highly effective, ensuring that models trained on this data reliably respond to the attacker’s intended inputs.

5.5 Ablation Study

In previous experiments, we used ConvNet as the attacker’s downstream model. In this experiment, we evaluate the impact of different model architectures on the effectiveness of our attack. To demonstrate the generalizability of our method, we conduct experiments on CIFAR-10 distilled using different DD methods, with IPC set to 10. The results, presented in Table 3, indicate that our attack remains highly effective across various model architectures. It can be seen that our threat model operates under relatively weak assumptions, making it highly practical in real-world scenarios. Despite these relaxed constraints, our attack maintains strong performance across various settings.

To further analyze the impact of different components in our method, we conduct an ablation study on the effect of α in Eq. (11), which balances the tradeoff between attack effectiveness and benign task performance. In this experiment, we use the CIFAR-10 dataset distilled by the DC method, with IPC set to 1. The results are

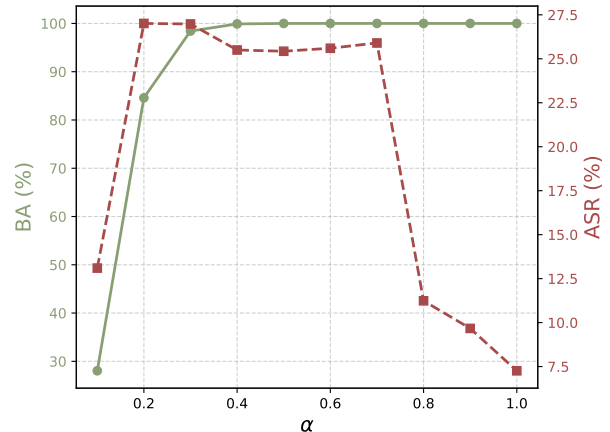


Figure 6: The performance under different α in Eq. (11).

Table 4: Computational complexity and attack performance with varying numbers of conceptual archetypes.

	Performance (%)		Time (s)		
	BA	ASR	Per Image	Per Epoch	All
$m = 5$	25.79	100.00	0.53	1.50	$0.53 \times 5 \times 10 + 1.50 \times 10 = 41.5$
$m = 10$	25.59	100.00	0.53	1.65	$0.53 \times 10 \times 10 + 1.65 \times 10 = 69.50$
$m = 20$	25.36	100.00	0.53	1.96	$0.53 \times 20 \times 10 + 1.96 \times 10 = 125.60$

shown in Figure 6. As α increases, ASR remains high, but the performance degradation on benign tasks becomes more pronounced. This occurs because a larger α emphasizes backdoor retention, potentially sacrificing the utility of the distilled dataset. To achieve an optimal balance between attack effectiveness and performance retention, we set α to 0.5 in our main experiments.

5.6 Computational Complexity

Our attack method is highly efficient and lightweight. To evaluate its computational cost, we conduct experiments on a CIFAR-10 dataset distilled by the DC method with IPC set to 1. The computational complexity varies based on the number of reconstructed conceptual archetypes, and the results are summarized in Table 4. It can be seen that different numbers of conceptual archetypes achieve effective attacks while maintaining minimal impact on benign performance. Therefore, we recommend using $m = 5$ as the default setting, as it provides a balance between efficiency and attack effectiveness.

The total attack time consists of two parts: conceptual archetype reconstruction and malicious distilled dataset synthesis. In the first phase, reconstructing each conceptual archetype requires only 0.53s, and under our default setting of five archetypes per class, this step takes approximately 26.5s for CIFAR-10. In the second phase, due to the small size of the distilled dataset, each epoch of synthesizing the malicious distilled dataset takes only 1.5 seconds on a single NVIDIA GTX 3090. Consequently, the entire attack can be completed in less than one minute. This minimal time overhead makes the attack virtually imperceptible to users, as they are unlikely to notice any delays that could suggest an ongoing attack.

6 Conclusion

In this paper, we propose a novel backdoor attack method targeting distilled datasets, which enables successful backdoor injection without requiring access to raw data, knowledge of the DD process,

or modifications to the data owner's pipeline. Our approach leverages the intrinsic properties of DD by reconstructing conceptual archetypes that align with the latent representations of real images, thereby bridging the gap between distilled and real data. We then embed backdoor information into the distilled dataset to ensure a consistent optimization trajectory with benign training, effectively concealing malicious behavior. Extensive experiments across various DD methods, raw datasets, training strategies, and downstream architectures demonstrate the effectiveness, generalizability, and stealthiness of our method. Our findings reveal a critical security vulnerability in dataset distillation, challenging the common belief that distilled datasets are inherently resistant to backdoor attacks [23]. We hope this work raises awareness of potential threats and encourages further research into defense mechanisms that ensure the security and trustworthiness of distilled datasets. In future work, we will develop defense algorithms to mitigate the proposed attack.

References

- [1] Tom Brown, Benjamin Mann, Nick Ryder, Melanie Subbiah, Jared D Kaplan, Prafulla Dhariwal, Arvind Neelakantan, Pranav Shyam, Girish Sastry, Amanda Askell, et al. 2020. Language models are few-shot learners. In *Advances in Neural Information Processing Systems*, Vol. 33. 1877–1901.
- [2] George Cazenavette, Tongzhou Wang, Antonio Torralba, Alexei A Efros, and Jun-Yan Zhu. 2022. Dataset distillation by matching training trajectories. In *Proceedings of the IEEE/CVF Conference on Computer Vision and Pattern Recognition*. 4750–4759.
- [3] Xinyun Chen, Chang Liu, Bo Li, Kimberly Lu, and Dawn Song. 2017. Targeted backdoor attacks on deep learning systems using data poisoning. *arXiv preprint arXiv:1712.05526* (2017).
- [4] Yilan Chen, Wei Huang, and Tsui-Wei Weng. 2024. Provable and Efficient Dataset Distillation for Kernel Ridge Regression. In *The Annual Conference on Neural Information Processing Systems*.
- [5] Ming-yu Chung, Sheng-yen Chou, Chia-Mu Yu, Pin-Yu Chen, Sy-yen Kuo, and Tsung-yi Ho. 2024. Rethinking Backdoor Attacks on Dataset Distillation: A Kernel Method Perspective. In *International Conference on Learning Representations*.
- [6] Justin Cui, Ruochen Wang, Si Si, and Cho-Jui Hsieh. 2023. Scaling up dataset distillation to imagenet-1k with constant memory. In *International Conference on Machine Learning*. PMLR, 6565–6590.
- [7] Tian Dong, Bo Zhao, and Lingjuan Lyu. 2022. Privacy for free: How does dataset condensation help privacy?. In *International Conference on Machine Learning*. PMLR, 5378–5396.
- [8] Jiawei Du, Qin Shi, and Joey Tianyi Zhou. 2024. Sequential subset matching for dataset distillation. *Advances in Neural Information Processing Systems* 36 (2024).
- [9] Jiawei Du, Xin Zhang, Juncheng Hu, Wenxin Huang, and Joey Tianyi Zhou. [n. d.]. Diversity-Driven Synthesis: Enhancing Dataset Distillation through Directed Weight Adjustment. In *The Thirty-eighth Annual Conference on Neural Information Processing Systems*.
- [10] Yu Feng, Benteng Ma, Jing Zhang, Shanshan Zhao, Yong Xia, and Dacheng Tao. 2022. Fiba: Frequency-injection based backdoor attack in medical image analysis. In *Proceedings of the IEEE/CVF Conference on Computer Vision and Pattern Recognition*. 20876–20885.
- [11] Tianyu Gu, Kang Liu, Brendan Dolan-Gavitt, and Siddharth Garg. 2019. Badnets: Evaluating backdooring attacks on deep neural networks. *IEEE Access* 7 (2019), 47230–47244.
- [12] Kaiming He, Xiangyu Zhang, Shaoqing Ren, and Jian Sun. 2016. Deep residual learning for image recognition. In *Proceedings of the IEEE conference on computer vision and pattern recognition*. 770–778.
- [13] Wenbo Jiang, Hongwei Li, Guowen Xu, and Tianwei Zhang. 2023. Color backdoor: A robust poisoning attack in color space. In *Proceedings of the IEEE/CVF Conference on Computer Vision and Pattern Recognition*. 8133–8142.
- [14] Diederik P Kingma and Jimmy Ba. 2014. Adam: A method for stochastic optimization. *arXiv preprint arXiv:1412.6980* (2014).
- [15] Alex Krizhevsky, Geoffrey Hinton, et al. 2009. Learning multiple layers of features from tiny images. (2009).
- [16] Alex Krizhevsky, Ilya Sutskever, and Geoffrey E Hinton. 2012. Imagenet classification with deep convolutional neural networks. *Advances in neural information processing systems* 25 (2012).
- [17] Alex Krizhevsky, Ilya Sutskever, and Geoffrey E Hinton. 2017. ImageNet classification with deep convolutional neural networks. *Commun. ACM* 60, 6 (2017), 84–90.
- [18] Yann LeCun, Yoshua Bengio, and Geoffrey Hinton. 2015. Deep learning. *nature* 521, 7553 (2015), 436–444.
- [19] Yann LeCun, Léon Bottou, Yoshua Bengio, and Patrick Haffner. 1998. Gradient-based learning applied to document recognition. *Proc. IEEE* 86, 11 (1998), 2278–2324.
- [20] Shiye Lei and Dacheng Tao. 2023. A comprehensive survey of dataset distillation. *IEEE Transactions on Pattern Analysis and Machine Intelligence* (2023).
- [21] Shiye Lei and Dacheng Tao. 2024. A Comprehensive Survey of Dataset Distillation. *IEEE Transactions on Pattern Analysis and Machine Intelligence* 46, 1 (2024), 17–32.
- [22] Yuezun Li, Yiming Li, Baoyuan Wu, Longkang Li, Ran He, and Siwei Lyu. 2021. Invisible backdoor attack with sample-specific triggers. In *Proceedings of the IEEE/CVF international conference on computer vision*. 16463–16472.
- [23] Yugeng Liu, Zheng Li, Michael Backes, Yun Shen, and Yang Zhang. 2023. Backdoor attacks against dataset distillation. In *Network and Distributed System Security (NDSS) Symposium*.
- [24] Noel Loo, Ramin Hasani, Alexander Amini, and Daniela Rus. 2022. Efficient dataset distillation using random feature approximation. *Advances in Neural Information Processing Systems* 35 (2022), 13877–13891.
- [25] Yuval Netzer, Tao Wang, Adam Coates, Alessandro Bissacco, Baolin Wu, Andrew Y Ng, et al. 2011. Reading digits in natural images with unsupervised feature learning. In *NIPS workshop on deep learning and unsupervised feature learning*, Vol. 2011. Granada, 4.
- [26] Tuan Anh Nguyen and Anh Tuan Tran. 2020. WaNet-Imperceptible Warping-based Backdoor Attack. In *International Conference on Learning Representations*.
- [27] Karen Simonyan and Andrew Zisserman. 2014. Very deep convolutional networks for large-scale image recognition. *arXiv preprint arXiv:1409.1556* (2014).
- [28] Peng Sun, Bei Shi, Daiwei Yu, and Tao Lin. 2024. On the diversity and realism of distilled dataset: An efficient dataset distillation paradigm. In *Proceedings of the IEEE/CVF Conference on Computer Vision and Pattern Recognition*. 9390–9399.
- [29] Laurens Van der Maaten and Geoffrey Hinton. 2008. Visualizing data using t-SNE. *Journal of machine learning research* 9, 11 (2008).
- [30] Tong Wang, Yuan Yao, Feng Xu, Shengwei An, Hanghang Tong, and Ting Wang. 2022. An invisible black-box backdoor attack through frequency domain. In *European Conference on Computer Vision*. Springer, 396–413.
- [31] Tongzhou Wang, Jun-Yan Zhu, Antonio Torralba, and Alexei A Efros. 2018. Dataset distillation. *arXiv preprint arXiv:1811.10959* (2018).
- [32] Han Xiao, Kashif Rasul, and Roland Vollgraf. 2017. Fashion-mnist: a novel image dataset for benchmarking machine learning algorithms. *arXiv preprint arXiv:1708.07747* (2017).
- [33] ShiMao Xu, Xiaopeng Ke, Xing Su, Shucheng Li, Hao Wu, Sheng Zhong, and Fengyuan Xu. 2024. Privacy-Preserving Federated Learning via Dataset Distillation. *arXiv preprint arXiv:2410.19548* (2024).
- [34] Zhe Xu, Yuzhong Chen, Menghai Pan, Huiyuan Chen, Mahashweta Das, Hao Yang, and Hanghang Tong. 2023. Kernel ridge regression-based graph dataset distillation. In *Proceedings of the ACM SIGKDD Conference on Knowledge Discovery and Data Mining*. 2850–2861.
- [35] Ziyuan Yang, Yingyu Chen, Mengyu Sun, and Yi Zhang. 2024. Inject Backdoor in Measured Data to Jeopardize Full-Stack Medical Image Analysis System. In *International Conference on Medical Image Computing and Computer-Assisted Intervention*. Springer, 393–402.
- [36] Ruonan Yu, Songhua Liu, and Xinchao Wang. 2023. Dataset distillation: A comprehensive review. *IEEE Transactions on Pattern Analysis and Machine Intelligence* (2023).
- [37] Ruonan Yu, Songhua Liu, Jingwen Ye, and Xinchao Wang. 2024. Teddy: Efficient large-scale dataset distillation via taylor-approximated matching. In *European Conference on Computer Vision*. Springer, 1–17.
- [38] Bo Zhao and Hakan Bilen. 2021. Dataset condensation with differentiable siamese augmentation. In *International Conference on Machine Learning*. PMLR, 12674–12685.
- [39] Bo Zhao and Hakan Bilen. 2023. Dataset Condensation with Distribution Matching. In *Proceedings of the IEEE/CVF Winter Conference on Applications of Computer Vision*.
- [40] Bo Zhao, Konda Reddy Mopuri, and Hakan Bilen. 2021. Dataset Condensation with Gradient Matching. In *International Conference on Learning Representations*.
- [41] Zhuangdi Zhu, Junyuan Hong, and Jiayu Zhou. 2021. Data-free knowledge distillation for heterogeneous federated learning. In *International conference on machine learning*. PMLR, 12878–12889.